

Simulation of phase separation in a Van der Waals fluid under gravitational force with Lattice Boltzmann method

Simulation of
phase
separation

3095

Ezequiel Oscar Fogliatto

*Comisión Nacional de Energía Atómica, Buenos Aires, Argentina and
Instituto Balseiro, Bariloche, Argentina*

Alejandro Clausse

*Comisión Nacional de Energía Atómica, Buenos Aires, Argentina,
National Council for Scientific and Technical Research, Buenos Aires,
Argentina and Universidad Nacional del Centro de la Provincia de Buenos Aires,
Tandil, Argentina, and*

Federico Eduardo Teruel

*Comisión Nacional de Energía Atómica, Buenos Aires, Argentina,
National Council for Scientific and Technical Research, Buenos Aires,
Argentina and Instituto Balseiro, Bariloche, Argentina*

Received 27 November 2018
Revised 15 January 2019
Accepted 12 February 2019

Abstract

Purpose – This paper aims to assess the accuracy of Lattice Boltzmann method (LBM) for numerical simulation of the stratification of a Van der Waals (VdW) fluid subjected to a gravity field and non-uniform temperature distribution. A sensitivity analysis of the influence of the pseudopotential parameters and the grid resolution is presented. The effect of gravity force on interface densities, density profiles and liquid volume fraction is studied.

Design/methodology/approach – The D2Q9 multiple-relaxation-time pseudopotential LBM for two-phase flow is proposed to simulate the phase separation. The analytical solution for density profiles in a one-dimensional problem is derived and used as a benchmark case to validate the numerical results.

Findings – The numerical results reproduce the analytical density profiles with great accuracy over a wide range of simulation conditions, including variations of the gravity and temperature fields. Particularly, the numerical simulations are able to represent the effect of gravity on the existence and position of the liquid–vapor boundary of an ideal pure substance in thermodynamic equilibrium. The sensitivity of the results to variations of the calibration parameters of the VdW pseudopotential was assessed.

Research limitations/implications – The numerical simulations were performed assuming a VdW fluid in a 2-D cavity with one periodic direction for which analytical solutions for benchmarking purposes are possible to obtain.

Originality/value – The following fundamental question is addressed: Is the pseudopotential LBM capable of simulating accurately the liquid–vapor equilibrium under gravity forces and temperature gradients? Moreover, regarding that the pseudopotential model requires the calibration of several internal



This work was supported by grants from Universidad Nacional de Cuyo (PB 2017-2019), from ANPCyT-FONCyT (PICT 201-0937 and 2016-0441), and from CONICET (PIP 112 201301-00829 CO).

International Journal of Numerical
Methods for Heat & Fluid Flow
Vol. 29 No. 9, 2019
pp. 3095-3109
© Emerald Publishing Limited
0961-5539
DOI 10.1108/HFF-11-2018-0682

parameters to achieve thermodynamic consistency, the sensitivity of the results to variations of these parameters is assessed.

Keywords Phase change, Gravity, Temperature gradient, Lattice Boltzmann method, Pseudopotential, Van der Waals

Paper type Research paper

Introduction

Multiphase flows are nearly ubiquitous in natural and industrial processes. Multiphase phenomena can involve single-component multiphase fluids, such as the water and vapor found in the primary loop of a nuclear reactor and multi-component multiphase fluids, such as the oil–gas–water found in the pipelines used for hydrocarbons transportation. Conventional computational methods discretize macroscopic governing equations and have been rather successfully applied to study specific multiphase systems. However, boiling phenomena involve mass, energy and momentum exchange processes between phases, which are quite complicated to model with conventional methods. In particular, the treatment of inertial interfacial coupling is still an open issue. All in all, simulation of multiphase flows often encountered in science and engineering is still a challenging task that has to overcome heavy obstacles such as the modeling of the interfacial behavior by tracking or capturing methods (Krüger *et al.*, 2017; Succi, 2001; Sun *et al.*, 2015).

Since its appearance more than two decades ago (Higuera and Jiménez, 1989; McNamara and Zanetti, 1988), the Lattice Boltzmann (LB) method has proved to be a reliable and viable numerical technique, capable of dealing with complex flows in a relatively simple and efficient way. Particularly, the straightforward parallelization of the resulting schemes is very attractive. From a physical point of view, the LB equation can be viewed as a minimal form of the transport Boltzmann equation in which the macroscopic kinetic principles are preserved to recover the hydrodynamic behavior at the macroscopic scale (Chen and Doolen, 1998; Succi, 2001). By means of this feature, the essential microscopic or mesoscopic physics can be incorporated in a direct fashion while recovering the macroscopic laws and properties at affordable computational cost (Li *et al.*, 2016).

The feasibility of Lattice Boltzmann method (LBM) for the numerical simulation of localized boiling phenomena has been recently showed by Sun (2015). Wettability effects in pool boiling were also studied using hybrid LBM (Gong and Cheng, 2015; Li *et al.*, 2015). Complex spatial patterns were also successfully simulated using LBM, like the mixing process due to Rayleigh–Taylor instability, which is similar to some interfacial phenomena (Liu and Guo, 2013; Tiribocchi *et al.*, 2011).

In general, multiphase LB models can be classified into one of the following categories: the color-gradient LB method (Gunstensen *et al.*, 1991), the free-energy LB method (Swift *et al.*, 1996), the phase-field LB method (He *et al.*, 1999), the kinetic method (Coclite *et al.*, 2014; Cristea *et al.*, 2006) and the pseudopotential LB method (Shan and Chen, 1994). The phase-field and pseudopotential methods have been successfully applied to multiphase flows at large density ratios and relatively high Reynolds numbers (Inamuro *et al.*, 2004; Lee and Lin, 2005; Li *et al.*, 2013, 2015; Zhao *et al.*, 2018), while the kinetic method has been used to study phase ordering in a Van der Waals (VdW) fluid under gravity (Cristea *et al.*, 2010). In the pseudopotential LB method, which is arguably the simplest, the fluid interactions are mimicked by an interparticle potential through which the separation of fluid phases or components can be achieved automatically without resorting to any techniques to track or capture interfaces (Sukop and Or, 2004). Indeed, it is remarkable that despite its apparent simplicity, this interaction force yields both, a non-monotonic equation of state (EOS)

supporting phase transition and non-zero surface tension. Therefore, the interface between different phases can arise, deform and migrate naturally (Succi, 2015).

The first version of the pseudopotential model was proposed by Shan and Chen (1994). However, this seminal model showed drawbacks regarding thermodynamic consistency, spurious currents and limitations in the values of the density and viscosity ratios to achieve stability (Benzi *et al.*, 2006; Chen *et al.*, 2014; He and Doolen, 2002). These problems motivated the development of improved forms of pseudopotentials with diverse success. Sbragaglia *et al.* (2007) introduced a multi-range potential and showed that when increasing the isotropy order of the discrete force operator, spurious currents can be significantly reduced. Kupershtokh *et al.* (2009) reported that a proper calculation of the interaction force can reduce thermodynamic inconsistency for the VdW EOS. Recently, Li *et al.* (2012) introduced an improved forcing scheme with a free parameter that can be tuned to approximately achieve thermodynamic consistency. Later on, this idea was extended by Li *et al.* (2013) to develop a two-dimensional nine-velocity (D2Q9) LB model with a multiple relaxation time (MRT) collision operator based on the aforementioned forcing scheme. This model controls the mechanical stability condition by means of a free parameter σ , and is capable of performing stable simulations with high density ratios ($\rho_l/\rho_g \sim 750$). Albeit this promising model was numerically validated for stationary and oscillating droplets and bubble departures from the wall in pool boiling (Fang *et al.*, 2017; Li *et al.*, 2013), the following fundamental question needs to be answered for any model developed to simulate multiphase flows: Is the model capable to accurately predict the liquid–vapor thermodynamic equilibrium under different thermodynamics conditions and gravity forces? To that end, the purpose of the present study is to address this issue exploring the capabilities of Li *et al.*'s LBM pseudopotential model (Li *et al.*, 2013) to represent the effect of gravity on the existence and position of the liquid–vapor boundary of an ideal pure substance in thermodynamic equilibrium. Moreover, regarding that the mentioned model requires the calibration of several internal parameters to achieve thermodynamic consistency, the sensitivity of the results to variations of these parameters will be assessed.

Multiple relaxation time pseudopotential model

The MRT-LBM is a more stable version than the original scheme that used a single-relaxation time. MRT has been applied successfully to many thermofluid flows (Li *et al.*, 2013, 2016). In the LB model, the evolution equation of the density distribution employing the MRT collision operator is described by:

$$f_\alpha(\mathbf{x} + \mathbf{e}_\alpha, t + \delta_t) = f_\alpha(\mathbf{x}, t) - \bar{\mathbf{A}}_{\alpha\beta} \left(f_\beta - f_\beta^{eq} \right) |_{(\mathbf{x},t)} + \delta_t (S_\alpha - 0.5 \bar{\mathbf{A}}_{\alpha\beta} S_\beta) |_{(\mathbf{x},t)} \quad (1)$$

where f_α is the density distribution function, f_α^{eq} is the equilibrium distribution, t is the time, \mathbf{x} is the spatial position, \mathbf{e}_α is the discrete velocity along the α -direction, δ_t is the time step and S_α is the forcing term in the velocity space. For the D2Q9 lattice, the collision matrix is defined as $\bar{\mathbf{A}} = \mathbf{M}^{-1} \mathbf{\Lambda} \mathbf{M}$, being \mathbf{M} an orthogonal transformation matrix and $\mathbf{\Lambda}$ a diagonal matrix given by (Li *et al.*, 2013):

$$\mathbf{\Lambda} = \text{diag} \left(\tau_\rho^{-1}, \tau_e^{-1}, \tau_s^{-1}, \tau_j^{-1}, \tau_q^{-1}, \tau_j^{-1}, \tau_q^{-1}, \tau_v^{-1}, \tau_v^{-1} \right) \quad (2)$$

The moment space can be obtained via the transformation matrix \mathbf{M} and the moment density distribution functions by $\mathbf{m} = \mathbf{M} \mathbf{f}$ and $\mathbf{m}^{eq} = \mathbf{M} \mathbf{f}^{eq}$. The equivalent to the right hand side of equation (1) can then be rewritten in the moment space as:

$$\mathbf{m}^* = \mathbf{m} - \Lambda(\mathbf{m} - \mathbf{m}^{eq}) + \delta_t \left(\mathbf{I} - \frac{\Lambda}{2} \right) \bar{\mathbf{S}} \tag{3}$$

where \mathbf{I} is the unitary tensor, $\bar{\mathbf{S}} = \mathbf{M}\mathbf{S}$ is the forcing term and the subscript $*$ denotes a post-collision stage. The streaming process is carried out employing the distribution function recovered from the Moment space with $\mathbf{f}^* = \mathbf{M}^{-1}\mathbf{m}^*$. Then, the macroscopic density and velocity are calculated by:

$$\rho = \sum_{\alpha} f_{\alpha}, \quad \rho\mathbf{v} = \sum_{\alpha} \mathbf{e}_{\alpha} f_{\alpha} + \frac{\delta_t}{2} \mathbf{F} \tag{4}$$

where $\mathbf{F} = (F_x, F_y) = \mathbf{F}_b + \mathbf{F}_{int}$ is the total force, \mathbf{F}_b is the body force and \mathbf{F}_{int} represents the interaction force acting on the system via an interaction potential $\psi(\mathbf{x})$:

$$\mathbf{F}_{int} = -G\psi(\mathbf{x}) \sum_{\alpha=1}^N w(|\mathbf{e}_{\alpha}|^2) \psi(\mathbf{x} + \mathbf{e}_{\alpha}) \mathbf{e}_{\alpha} \tag{5}$$

In [equation \(5\)](#), G is the interaction strength and $w(|\mathbf{e}_{\alpha}|^2)$ are the weights corresponding to the D2Q9 Lattice. The modified pseudopotential model ([Li et al., 2013](#)) corrects the forcing scheme given in the MRT version by [Guo et al. \(2002\)](#) to compensate for the thermodynamic inconsistency problem. Due to this inconsistency the LB model yields erroneous values of the liquid and vapor densities at the interface ([Guo et al., 2002](#); [Kupershtokh et al., 2009](#)) on the score of failing to comply with the Maxwell's equal-area rule ([Huang et al., 2015](#)):

$$\int_{\rho_g}^{\rho_l} (p_0 - p_{EOS}) \frac{1}{\rho^2} d\rho = 0 \tag{6}$$

where p_{EOS} is the EOS in the thermodynamic theory and $p_0 = p_{EOS}(\rho) = p_{EOS}(\rho_g)$, with ρ_l and ρ_g densities of the liquid and solid phases respectively. The improved forcing scheme of [Li et al.](#) is given by:

$$\bar{\mathbf{S}} = \begin{bmatrix} 0 \\ 6u \cdot \mathbf{F} + \frac{12 \sigma |\mathbf{F}_{int}|^2}{\psi^2 \delta_t (\tau_e - 0.5)} \\ -6u \cdot \mathbf{F} - \frac{12 \sigma |\mathbf{F}_{int}|^2}{\psi^2 \delta_t (\tau_s - 0.5)} \\ F_x \\ -F_x \\ F_y \\ -F_y \\ 2(v_x F_x - v_y F_y) \\ (v_x F_y + v_y F_x) \end{bmatrix} \tag{7}$$

The source given by [equation \(7\)](#) introduces a free parameter that can be used to approximately achieve thermodynamic consistency. For the special case of $\sigma = 0$ the new

forcing scheme reduces to the version of the forcing scheme of (Guo *et al.*, 2002). Moreover, for a flat interface the normal pressure is calculated from the discrete form of the pressure tensor (Shan, 2008) as:

$$P_n = \rho c_s^2 + \frac{Gc^2}{2} \psi^2 + \frac{Gc^4}{12} \left[\alpha \left(\frac{d\psi}{dn} \right)^2 + \beta \psi \frac{d^2\psi}{dn^2} \right] \quad (8)$$

where n is the direction normal to the interface and $\alpha = 0$ and $\beta = 3$ for the case of first neighbor interaction. Therefore, the mechanical stability condition satisfied by the LB simulation is equivalent to the Maxwell's rule, provided that P_n is equal to the static pressure at equilibrium in the bulk (Shan, 2008), that is:

$$\int_{\rho_g}^{\rho_l} \left(p_0 - \rho c_s^2 - \frac{Gc^2}{2} \psi^2 \right) \frac{\psi'}{\psi^{1+\epsilon}} d\rho = 0 \quad (9)$$

where $\psi' = d\psi/d\rho$ and $\epsilon = -2\alpha/\beta$. Thus, it is clear that the Maxwell's equal-area rule [equation (6)] cannot be satisfied if a general EOS is employed in the pseudopotential definition:

$$\psi(\rho) = \sqrt{\frac{2(p_{EOS} - \rho c_s^2)}{Gc^2}} \quad (10)$$

because, in general, $\psi'/\psi^{1+\epsilon} \neq 1/\rho^2$ in the mechanical stability condition given by equation (9). With the modified forcing scheme given by equation (7), the equivalent to equation (8) is given by (Li *et al.*, 2012):

$$P_n = \rho c_s^2 + \frac{Gc^2}{2} \psi^2 + \frac{Gc^4}{12} \left[(\alpha + 24G\sigma) \left(\frac{d\psi}{dn} \right)^2 + \beta \psi \frac{d^2\psi}{dn^2} \right] \quad (11)$$

Note that equation (11) equals equation (8) if $\epsilon = -2(\alpha + 24G\sigma)/\beta$. Therefore, the free parameter can be employed to approximately ensure that the numerical simulation is thermodynamically consistent. That is, for a given EOS and a given liquid–vapor interface problem, we can make the integrand of equation (9) approximately equal to that in equation (6). In practice, if the equilibrium densities are known at the vapor-liquid interface, consistency can be approximately achieved calibrating the value of σ to match these known values with the LB results.

Gravitational stratification of a Van der Waals fluid

Berberan-Santos *et al.* (2002) provided a useful case study of vapor-liquid stratification of a VdW fluid in a tall isothermal container subjected to a gravitational field for which a first-order ordinary differential equation can be obtained. Here, we present an extension of the mentioned analysis including an arbitrary temperature profile along the vertical direction, y . The pressure gradient in y is determined by the hydrostatic balance as:

$$\frac{dP}{dy} = -gM\rho_m \quad (12)$$

where P is the pressure, g is the gravity acceleration, M is the molecular weight, and ρ_m is the molar density. The pressure is related to the density and the temperature T by the EOS of a VdW fluid:

$$P = \frac{RT\rho_m}{1 - b\rho_m} - a\rho_m^2 \quad (13)$$

where R is the gas constant, and a and b are the VdW parameters. Combining equations (12) and (13) gives:

$$\frac{d\rho_m}{dy} = -\frac{Mg\rho_m + \frac{dT}{dy} \left(\frac{R\rho_m}{1 - b\rho_m} \right)}{\frac{RT}{(1 - b\rho_m)^2} - 2a\rho_m} \quad (14)$$

The boundary condition for equation (14) is the gas-liquid interface, which is determined by the total mass in the container and the temperature profile. At the interface, the pressure and the Gibbs free energy are the same for liquid and gas, which leads to:

$$P_{sat} = \frac{RT\rho_g}{1 - b\rho_g} - a\rho_g^2 = \frac{RT\rho_l}{1 - b\rho_l} - a\rho_l^2 \quad (15)$$

$$T \ln \left(\frac{\rho_g^{-1} - b}{\rho_l^{-1} - b} \right) + a(\rho_g - \rho_l) = P_{sat} \left(\frac{1}{\rho_g} - \frac{1}{\rho_l} \right) \quad (16)$$

where ρ_l and ρ_g are the molar liquid and gas saturated densities respectively, and P_{sat} is the saturation pressure. The equations (15) and (16) determine the equilibrium values ρ_g and ρ_l at the interface for a given temperature T . Integrating now equation (14) from the interface at $y = y_o$ and a generic y , gives the density profiles of the liquid phase $\rho_m^-(y)$ for $y < y_o$ and the vapor phase $\rho_m^+(y)$ for $y > y_o$. The total number of moles N in the vessel is then given by:

$$N = \int_0^{y_o} \rho_m^-(y) dy + \int_{y_o}^H \rho_m^+(y) dy \quad (17)$$

Thus, given an initial number of moles, the position of the interface y_o can be determined with equation (17). Finally, the molar density profiles $\rho_m^-(y)$ and $\rho_m^+(y)$ are obtained, which provides a golden standard to test the pseudopotential LB model. In the next section this profiles are compared with the pseudopotential LB numerical simulations.

Results

The MRT-LB scheme of Li *et al.* (2013), given by equations (1), (3), (4), (5) and (10), was implemented in a 2-D grid of $L = 3$ lattice nodes in the horizontal direction and $H = 3000$ lattice nodes in the vertical direction, as schematically shown in Figure 1. The boundary conditions in each direction, width and height, are periodic and bounce-back, respectively. The values of the fixed parameters from the VdW EOS used throughout all the simulations are $G = -1$, $R = 1$, $a = 0.5$ and $b = 4.0$. Otherwise stated, the relaxation parameters are chosen to be $\tau_\rho = \tau_j = 1.0$ and $\tau_e^{-1} = \tau_s^{-1} = \tau_v^{-1} = \tau_q^{-1} = 1.1$. The value of the parameter σ was left free to calibrate the model for a VdW fluid.

In the first numerical test no gravitational forces are imposed, and the goal is to determine the value of σ that best approximates the interface densities determined by the

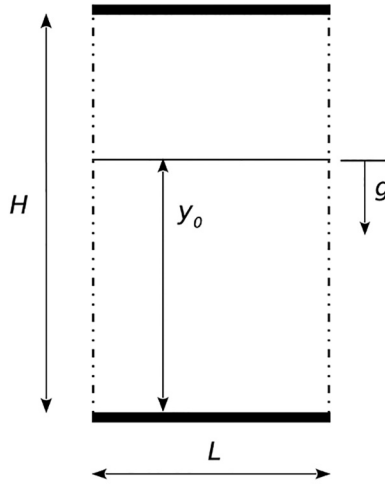


Figure 1.
Schematic view of the
domain employed in
the LB simulations

VdW EOS with $a = 0.5$ and $b = 4$. The column density is initially set randomly within a $\pm 1\%$ around the critical value. The temperature of the system is fixed in every run at a reduced value in the range between 0.5 and 1. When the steady state is reached, the density across the domain splits up into two values, corresponding to the gas-liquid equilibrium. **Figure 2** shows the two-phase bell resulting from plotting the reduced density $\rho_r = \rho/\rho_c$ of the liquid and gas phase for each equilibrium temperature. The theoretical curve corresponding to the VdW EOS calculated using [equations \(15\)](#) and [\(16\)](#) is also shown in **Figure 2**. It can be seen that the proposed LBM scheme with $\sigma = 1/8$ produces an excellent approximation in a wide range of temperatures. Moreover, as originally pointed out by [Li et al. \(2013\)](#), our simulations show that the coexistence curves from **Figure 2** show no significant changes when different values of τ_v are used.

In the second numerical test, an external gravitational force is applied in the vertical direction of the domain with constant and uniform reduced temperature T_r , i.e. T divided by the critical temperature. The parameter σ is fixed in $1/8$. The value of the gravitational force is determined by the dimensionless number:

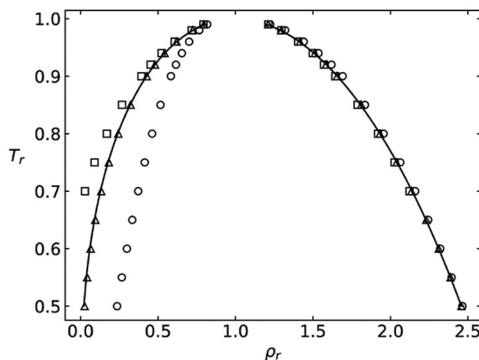


Figure 2.
Locus of phase
coexistence at
thermodynamic
equilibrium for a
VdW fluid ($a = 0.5$,
 $b = 4$). The symbols
corresponds to the
numerical simulation
with $\sigma = 1.25$ (\circ),
 0.125 (\triangle), 0.0125 (\square).
The curve
corresponds to the
exact locus

$$E_r = \frac{MgH}{RT_c} = 0.001 \tag{18}$$

As expected by hydrostatics the liquid phase occupies the lower part of the domain. In turn, the density is uniform in the horizontal coordinate. Figure 3 shows the density profile along the vertical coordinate for different reduced temperatures. Lower temperatures lead to greater density differences between phases, which is in agreement with Figure 2. Figure 4 shows the dependence of the position of the interface with the temperature for different average densities. It can be seen that for the critical density the interface approaches the center of the domain ($y/H = 0.5$) as the critical temperature approaches unity. On the other hand, Figure 5 compares density profiles for $T_r = 0.99$ and $\sigma = 1/8$ over a wide range of E_r . It can be seen that the same value of σ can be used to correctly take into account the effects of gravitational forces.

The third case is similar to the second test, i.e., $\sigma = 1/8$ and an external gravitational force applied along the y coordinate [equation (18)]. A lineal temperature profile is imposed

Figure 3. Density spatial profile when applying a gravity field in the y (vertical) direction to an isothermal domain. The intensity of the gravity field is given by $E_r = 0.001$. The symbols are the analytical solution given by equation (14) with $T_r = 0.5$ (\circ), 0.7 (\triangle), 0.99 (\square). The curves are the corresponding numerical results obtained with $\sigma = 1/8$

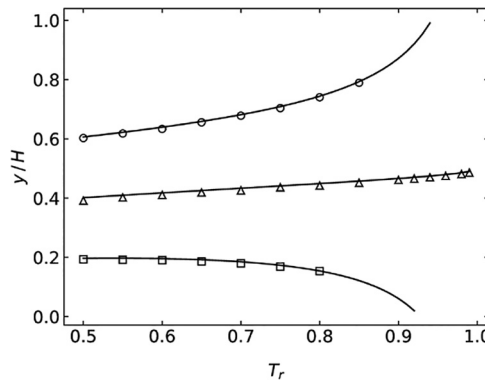
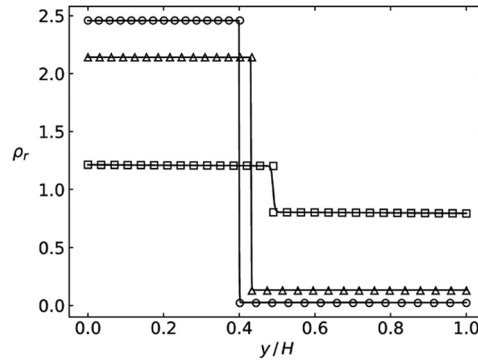


Figure 4. Dependence of the interface position with the equilibrium temperature for different average densities, namely $\rho_r = 1.5$ (\circ), 1.0 (\triangle), 0.5 (\square)

along the y coordinate, with $T_r = 0.99$ at $y=H$, and a fixed parametric value at $y=0$. Figure 6 compares the density profiles given by equation (14) with the numerical simulations. It is worth noting that the spatial resolution plays an important role in the accuracy of the approximation. Figures 7 and 8 show the density profiles simulated with different number of lattice nodes along the vertical direction, for the cases of constant temperature and constant temperature gradient, respectively. It can be seen that the agreement with the analytical solution weakens as the spatial resolution decreases. This expected effect is more salient closer to the critical point.

VdW EOS constants also play an important role in the accuracy of simulations to describe the density profile across the interface. Figures 9 and 10 show density distributions in an isothermal container obtained with $T_r = 0.8$, fixed b with varying a , and fixed a with varying b respectively. It can be seen that both, increasing a or decreasing b , reduce the

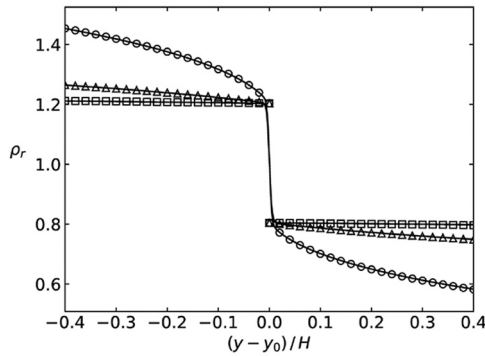


Figure 5. Density profiles for $T_r = 0.99$ and $\sigma = 1/8$ and different dimensionless numbers $E_r = 0.1$ (\circ), 0.01 (\triangle), 0.001 (\square). Solid curves are the corresponding numerical results

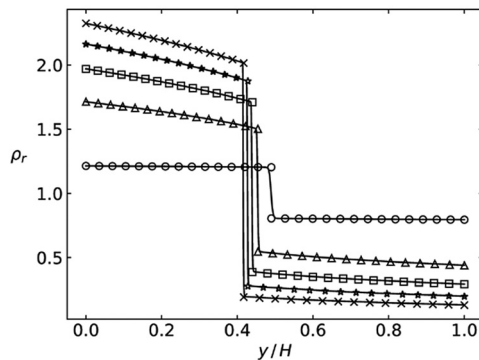


Figure 6. Density spatial profile when applying a constant gravity field and a constant temperature gradient. The intensity of the gravity field is given by $E_r = 0.001$. The reduced temperature at $y = H$ is fixed in 0.99 . The symbols are the analytical solution given by equation (14) with a temperature at $y = 0$, $T_r(0) = 0.6$ (\times), 0.7 (\ast), 0.8 (\square), 0.9 (\triangle), 0.99 (\circ). The curves are the corresponding numerical results obtained with $\sigma = 1/8$

interface width, similar to what is found when increasing the grid resolution (Figures 7 and 8). Therefore, these two constants may be employed to improve accuracy without changing the grid resolution.

Numerical results show that the LB model is capable of reproducing density profiles given by the analytical solution under different simulation conditions. The parameter σ can be freely tuned to approximately achieve thermodynamic consistency, thus obtaining an excellent agreement away from the interface and a continuum profile where segregation takes place. Moreover, the interface width can be further improved, for instance, refining the grid. This behavior can be analyzed as a result of the recovered Navier-Stokes equation (Li *et al.*, 2013):

Figure 7.

Sensitivity of the density profile with the spatial resolution. Isothermal domain ($T_r = 0.99$) with $E_r = 0.001$. The symbols show the analytical solution. The curves are the corresponding numerical results obtained with $\sigma = 1/8$ with different number of lattice units in the vertical direction

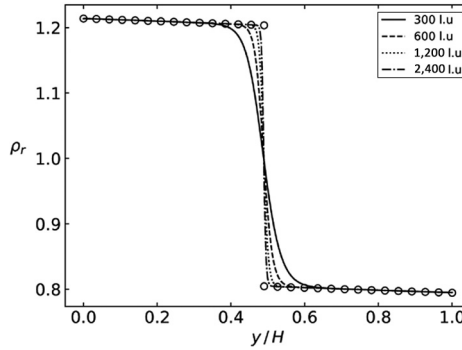
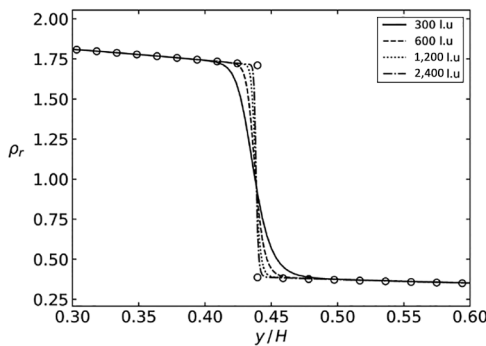


Figure 8.

Sensitivity of the density profile with the spatial resolution. Gravity by $E_r = 0.001$, and constant temperature gradient given by $T_r(H) = 0.99$, $T_r(0) = 0.9$. The symbols show the analytical solution. The curves are the corresponding numerical results obtained with $\sigma = 1/8$ with different number of lattice nodes in the vertical direction



$$\frac{\partial}{\partial t}(\rho \mathbf{u}) + \nabla \cdot (\rho \mathbf{u} \mathbf{u}) = -\nabla \cdot (\rho c_s^2 I) + \nabla \cdot \mathbf{\Pi} + \mathbf{F} - 2G^2 c^4 \sigma \nabla \cdot (|\nabla \psi|^2 I) + O(\partial^5) \quad (19)$$

Simulation of
phase
separation

where $\mathbf{\Pi}$ is the viscous stress tensor and \mathbf{F} the total force which can be expressed as (Shan, 2008):

$$\mathbf{F} = -Gc^2 \left[\psi \nabla \psi + \frac{1}{6} c^2 \psi \nabla (\nabla^2 \psi) + \dots \right] + \mathbf{F}_b = \mathbf{F}_{int} + \mathbf{F}_b \quad (20)$$

For our one-dimensional case, equation (19) can be reduced to:

$$-\frac{\partial}{\partial y} (\rho c_s^2) + F_{int_y} + F_{b_y} - 2G^2 c^4 \sigma \frac{\partial}{\partial y} \left(\left| \frac{\partial \psi}{\partial y} \right|^2 \right) + O(\partial^5) = 0 \quad (21)$$

3105

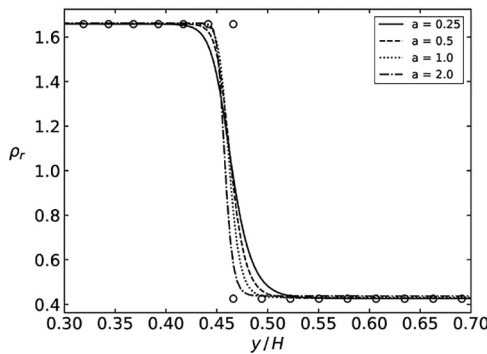


Figure 9.
Sensitivity of the
density profile with
VdW EOS constant a .
Isothermal domain
with $T_r = 0.8$ and
 $E_r = 10^{-3}$. The
symbols show the
analytical solution.
The curves are the
corresponding
numerical results
obtained with $\sigma = 1/8$
and $b = 4$

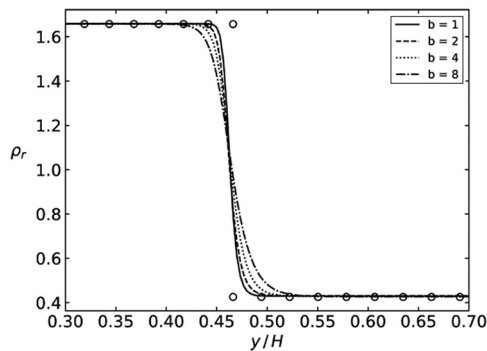


Figure 10.
Sensitivity of the
density profile with
VdW EOS constant b .
Isothermal domain
with $T_r = 0.8$ and
 $E_r = 10^{-3}$. The
symbols show the
analytical solution.
The curves are the
corresponding
numerical results
obtained with $\sigma = 1/8$
and $a = 0.5$

Figure 11 shows the profiles of the interaction force and $\psi d\psi/dy$ for an isothermal container with $T_r = 0.99$, $E_r = 10^{-3}$ and 300 lattice units. Note that since the interaction force satisfies $F_{int_y} = -Gc^2 \psi d\psi/dy$, then equation (21) can be further reduced using equation (10) as follows:

$$-\frac{\partial p_{EOS}}{\partial y} + F_{b_y} - 2G^2c^4\sigma \frac{\partial}{\partial y} \left(\left| \frac{\partial \psi}{\partial y} \right|^2 \right) = 0 \quad (22)$$

The equation (22) is similar to the hydrostatic force balance employed by Berberan–Santos (equation (12)) except for the additional term $-2G^2c^4\sigma \frac{\partial}{\partial y} \left(\left| \frac{\partial \psi}{\partial y} \right|^2 \right)$. Figure 12 shows the importance of different terms in equation (21). Although equation (21) is similar to

Figure 11.

Axial profiles of the interaction force (curve) and $\psi \partial_y \psi$ (symbols) with gravity given by $E_r = 0.001$, and constant temperature gradient given by $T_r = 0.99$. $\psi \partial_y \psi$ was computed using equation (10) and finite difference schemes for the spatial derivative

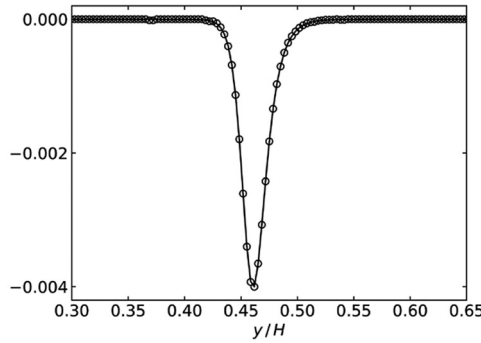
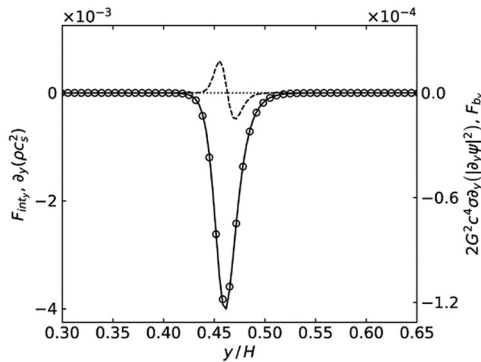


Figure 12.

Spatial profile of different terms of equation (21), obtained from a simulation of an isothermal container with $T_r = 0.99$ and gravity field given by $E_r = 0.001$. The curves correspond to F_{int_y} (solid line), $\partial_y(\rho c_s^2)$ (symbol), $2G^2c^4\sigma \frac{\partial}{\partial y} \left(\left| \partial_y \psi \right|^2 \right)$ (dashed line) and F_{b_y} (dotted line)



equation (12) in almost the entire domain, $-2G^2c^4\sigma\frac{\partial}{\partial y}\left(\left|\frac{\partial}{\partial y}\psi\right|^2\right)$ becomes non-zero in the vicinities of the interface, and despite being one order of magnitude smaller than the leading terms of equation (21), it can affect macroscopic variables so as to produce the observed continuum and diffuse density profiles across the interface.

Conclusion

In this paper, a LB simulation of stratification of a VdW fluid in a closed vessel subjected to gravity field has been presented. The LB results were compared against an analytical solution for density profiles in a one-dimensional problem, and this solution has been extended to include temperature variations in the spatial coordinate. Results show that the tested MRT – pseudopotential LB model of Li *et al.* can precisely reproduce density profiles over a wide range of simulation conditions, including gravity field magnitude and domain temperature. Although the comparison in the present study was performed against a one-dimensional analytical solution, we remark that the numerical experiments were carried out in a two dimensional domain. In this regard, it was verified that the numerical solution is independent on the size of the horizontal span of the domain for a fixed resolution, and only dependent on the vertical coordinate. The calibration of model parameters to achieve thermodynamic consistency was carried out for the VdW EOS with a fixed set of EOS constants and zero gravitational forces. This calibration was found to be fairly independent of simulation conditions providing excellent results for a variety of cases with gravity forces and temperature profiles. It was also observed that the analytical solution and its extension can provide a simple but reliable benchmark case to test specific features of multiphase LB models, such as approximate thermodynamic consistency and grid independence studies.

References

- Benzi, R., Biferale, L., Sbragaglia, M., Succi, S. and Toschi, F. (2006), “Mesoscopic modeling of a two-phase flow in the presence of boundaries: the contact angle”, *Physical Review E*, Vol. 74, No. 2 p. 021509.
- Berberan-Santos, M.N., Bodunov, E.N. and Pogliani, L. (2002), “Liquid–vapor equilibrium in a gravitational field”, *American Journal of Physics*, Vol. 70 No. 4, p. 438.
- Chen, L., Kang, Q., Mu, Y., He, Y.-L. and Tao, W.-Q. (2014), “A critical review of the pseudopotential multiphase lattice Boltzmann model: methods and applications”, *International Journal of Heat and Mass Transfer*, Vol. 76, pp. 210-236.
- Chen, S. and Doolen, G.D. (1998), “Lattice Boltzmann method for fluid flows”, *Annual Review of Fluid Mechanics*, Vol. 30 No. 1, pp. 329-364.
- Coclite, A., Gonnella, G. and Lamura, A. (2014), “Pattern formation in liquid-vapor systems under periodic potential and shear”, *Physical Review E*, Vol. 89, No. 6, p. 063303.
- Cristea, A., Gonnella, G., Lamura, A. and Sofonea, V. (2006), “Finite-difference Lattice Boltzmann model for liquid–vapor systems”, *Mathematics and Computers in Simulation*, Vol. 72 Nos 2/6, pp. 113-116.
- Cristea, A., Gonnella, G., Lamura, A. and Sofonea, V. (2010), “A Lattice Boltzmann study of phase separation in liquid-vapor systems with gravity”, *Communications in Computational Physics*, Vol. 7, pp. 350-361.
- Fang, W.-Z., Chen, L., Kang, Q.-J. and Tao, W.-Q. (2017), “Lattice Boltzmann modeling of pool boiling with large liquid-gas density ratio”, *International Journal of Thermal Sciences*, Vol. 114, pp. 172-183.

- Gong, S. and Cheng, P. (2015), "Lattice Boltzmann simulations for surface wettability effects in saturated pool boiling heat transfer", *International Journal of Heat and Mass Transfer*, Vol. 85, pp. 635-646.
- Gunstensen, A.K., Rothman, D.H., Zaleski, S. and Zanetti, G. (1991), "Lattice Boltzmann model of immiscible fluids", *Physical Review A*, Vol. 43 No. 8, p. 4320.
- Guo, Z., Zheng, C. and Shi, B. (2002), "Discrete Lattice effects on the forcing term in the Lattice Boltzmann method", *Physical Review E*, Vol. 65 No. 4, p. 046308.
- He, X., Chen, S. and Zhang, R. (1999), "A Lattice Boltzmann scheme for incompressible multiphase flow and its application in simulation of Rayleigh–Taylor instability", *Journal of Computational Physics*, Vol. 152 No. 2, pp. 642-663.
- He, X. and Doolen, G.D. (2002), "Thermodynamic foundations of kinetic theory and Lattice Boltzmann models for multiphase flows", *Journal of Statistical Physics*, Vol. 107 Nos 1/2, pp. 309-328.
- Higuera, F.J. and Jiménez, J. (1989), "Boltzmann approach to Lattice gas simulations", *Europhysics Letters (EPL)*, Vol. 9 No. 7, pp. 663-668.
- Huang, H., Sukop, M.C. and Lu, X.-Y. (2015), *Multiphase Lattice Boltzmann Methods: theory and Application*, John Wiley and Sons, Chichester, West Sussex.
- Inamuro, T., Ogata, T., Tajima, S. and Konishi, N. (2004), "A Lattice Boltzmann method for incompressible two-phase flows with large density differences", *Journal of Computational Physics*, Vol. 198 No. 2, pp. 628-644.
- Krüger, T., Kusumaatmaja, H., Kuzmin, A., Shardt, O., Silva, G. and Viggen, E.M. (2017), *The Lattice Boltzmann Method – Principles and Practice, Graduate Texts in Physics*, Springer International, New York, NY.
- Kupershtokh, A.L., Medvedev, D.A. and Karpov, D.I. (2009), "On equations of state in a Lattice Boltzmann method", *Computers and Mathematics with Applications*, Vol. 58, pp. 965-974.
- Lee, T. and Lin, C.-L. (2005), "A stable discretization of the Lattice Boltzmann equation for simulation of incompressible two-phase flows at high density ratio", *Journal of Computational Physics*, Vol. 206 No. 1, pp. 16-47.
- Li, Q., Kang, Q.J., Francois, M.M., He, Y.L. and Luo, K.H. (2015), "Lattice Boltzmann modeling of boiling heat transfer: the boiling curve and the effects of wettability", *International Journal of Heat and Mass Transfer*, Vol. 85, pp. 787-796.
- Li, Q., Luo, K.H., Kang, Q.J., He, Y.L., Chen, Q. and Liu, Q. (2016), "Lattice Boltzmann methods for multiphase flow and phase-change heat transfer", *Progress in Energy and Combustion Science*, Vol. 52, pp. 62-105.
- Li, Q., Luo, K.H. and Li, X.J. (2012), "Forcing scheme in pseudopotential Lattice Boltzmann model for multiphase flows", *Physical Review E*, 86 No. 1, p. 016709.
- Li, Q., Luo, K.H. and Li, X.J. (2013), "Lattice Boltzmann modeling of multiphase flows at large density ratio with an improved pseudopotential model", *Physical Review E*, Vol. 87, p. 053301.
- Li, Z., Yang, M. and Zhang, Y. (2016), "Double MRT thermal Lattice Boltzmann method for simulating natural convection of low prandtl number fluids", *International Journal of Numerical Methods for Heat and Fluid Flow*, Vol. 26, pp. 1889-1909.
- Liu, G. and Guo, Z. (2013), "Effects of prandtl number on mixing process in miscible Rayleigh-Taylor instability: a Lattice Boltzmann study", *International Journal of Numerical Methods for Heat and Fluid Flow*, Vol. 23, pp. 176-188.
- McNamara, G.R. and Zanetti, G. (1988), "Use of the Boltzmann equation to simulate Lattice-gas automata", *Physical Review Letters*, Vol. 61 No. 20, p. 2332.
- Sbragaglia, M., Benzi, R., Biferale, L., Succi, S., Sugiyama, K. and Toschi, F. (2007), "Generalized Lattice Boltzmann method with multirange pseudopotential", *Physical Review E*, Vol. 75. No. 2, p. 026702.

-
- Shan, X. (2008), "Pressure tensor calculation in a class of nonideal gas Lattice Boltzmann models", *Physical Review E* 77.
- Shan, X. and Chen, H. (1994), "Simulation of nonideal gases and liquid-gas phase transitions by the Lattice Boltzmann equation", *Physical Review E, Statistical Physics, Plasmas, Fluids, and Related Interdisciplinary Topics*, Vol. 49 No. 4, p. 2941.
- Succi, S. (2001), *The Lattice Boltzmann Equation for Fluid Dynamics and beyond, Numerical Mathematics and Scientific Computation*, Oxford University Press, Oxford.
- Succi, S. (2015), "Lattice Boltzmann 2038", *EPL (Europhysics Letters)*, Vol. 109 No. 5, p. 50001.
- Sukop, M.C. and Or, D. (2004), "Lattice Boltzmann method for modeling liquid-vapor interface configurations in porous media: Lattice Boltzmann for interface configurations", *Water Resources Research* 40.
- Sun, T., Li, W. and Dong, B. (2015), "Numerical simulation of vapor bubble growth on a vertical superheated wall using Lattice Boltzmann method", *International Journal of Numerical Methods for Heat and Fluid Flow*, Vol. 25, pp. 1214-1230.
- Swift, M.R., Orlandini, E., Osborn, W.R. and Yeomans, J.M. (1996), "Lattice Boltzmann simulations of liquid-gas and binary fluid systems", *Physical Review E*, Vol. 54 No. 5, p. 5041.
- Tiribocchi, A., Piscitelli, A., Gonnella, G. and Lamura, A. (2011), "Pattern study of thermal phase separation for binary fluid mixtures", *International Journal of Numerical Methods for Heat and Fluid Flow*, Vol. 21, pp. 572-583.
- Zhao, X., Dong, B. and Li, W. (2018), "Analysis of freezing process about falling droplet using the Lattice Boltzmann method", *International Journal of Numerical Methods for Heat and Fluid Flow*, Vol. 28, pp. 2442-2462.

Corresponding author

Ezequiel Fogliatto can be contacted at: fogliatto@cab.cnea.gov.ar

For instructions on how to order reprints of this article, please visit our website:

www.emeraldgrouppublishing.com/licensing/reprints.htm

Or contact us for further details: permissions@emeraldinsight.com